IEEE Access
Multidisciplinary ⋮ Rapid Review ⋮ Open Access Journal

Received August 26, 2020, accepted September 3, 2020, date of publication September 7, 2020,
date of current version September 22, 2020.

Digital Object Identifier 10.1109/ACCESS.2020.3022389

Sensitive Relative Humidity Monitoring Sensor Based on Microwave Active Resonator With PEDOT:PSS

JIN-KWAN PARK[1], (Graduate Student Member, IEEE), CHOROM JANG[1], (Graduate Student Member, IEEE), GI-HO YUN[2], HEE-JO LEE[3], (Member, IEEE), HYANG HEE CHOI[4], AND JONG-GWAN YOOK[1], (Senior Member, IEEE)

[1]Department of Electrical and Electronics Engineering, Yonsei University, Seoul 03722, South Korea
[2]Department of Information and Communications Engineering, Sungkyul University, Anyang 14097, South Korea
[3]Department of Physics Education, Daegu University, Gyeongsan 38453, South Korea
[4]Institute of Engineering Research, Yonsei University, Seoul 03722, South Korea

Corresponding author: Jong-Gwan Yook (jgyook@yonsei.ac.kr)

This work was supported by the National Research Foundation of Korea (NRF), through the Basic Science Research Program, funded by the Ministry of Science and ICT under Grant NRF-2017R1A2B2011724.

ABSTRACT In this paper, a relative humidity monitoring sensor based on an active resonator with PEDOT:PSS is studied in the microwave regime. The proposed active resonator is patterned on a printed circuit board and excited by electromagnetic field coupling. The active resonator consists of two parts: a passive core resonator and an active circuit. The passive core resonator senses the humidity via the PEDOT:PSS conducting polymer film, which is located in the area of the passive core resonator with the strongest electric field. The active circuit compensates for the loss of the passive core resonator to enhance the quality factor and thus improve the sensitivity of the relative humidity sensor. By combining the passive core resonator with the active circuit, the active resonator exhibits a high quality factor (2887), which is 90 times that of the passive core resonator alone. Moreover, the sensitivity of the proposed humidity sensor is improved when using the active resonator. To verify the performance of the proposed humidity sensor, a commercial sensor is placed alongside the proposed sensor in a well-controlled environment chamber. According to the experimental results, as the relative humidity increases, the transmission coefficient (S_{21}) increases, while the resonance frequency decreases. As a result, the sensor exhibits an increase in S_{21} of 3.58 dB and a decrease in the resonance frequency of 8.85 MHz when the relative humidity changes from 30% to 85%.

INDEX TERMS Active resonator, humidity sensor, PEDOT:PSS, conducting polymer, radio frequency, real-time sensing.

I. INTRODUCTION

Poly(3,4-ethylenedioxythiophene):polystyrene sulfonate (PEDOT:PSS), an organic conducting polymer, is a promising material because of its outstanding properties, such as high conductivity, low price, room temperature operation, low redox potential and good processability [1], [2]. For these reasons, most previous studies used PEDOT:PSS as a sensing material for gas [3] and humidity [4] sensing. However, most of the studies are based on field effect transistors (FETs) [5] or electrode-based sensors [6]. These sensors can only measure one parameter, such as changes in the voltage, current, or resistance. This means that the information obtained from the measurement is very limited. Moreover, these sensors are difficult to fabricate, and enhancing their sensitivity is also challenging. Therefore, to overcome these problems, several types of research have recently been conducted with PEDOT:PSS-based sensors operating in the microwave regime [7].

First, microwave sensors are suitable for noninvasive, nondestructive and noncontact measurements [8]–[10]. Moreover, their size can be reduced by increasing the operating frequency, and they can be easily incorporated into commercial mobile communication systems [11], [12]. Among the

The associate editor coordinating the review of this manuscript and approving it for publication was Mohamed Kheir.

microwave components, planar microstrip resonators have been widely used as sensing platforms due to their simple fabrication process, ease of portability, small volume and low cost. Despite these advantages, planar microstrip resonator-based sensors require further enhancement of their low quality factor, which is closely related to the resolution of the sensor. A low quality factor means that a considerable amount of energy is dissipated in the resonator, which decreases the reactivity with the material of interest. Because of these properties, detecting lossy materials or dielectric materials with a high dielectric constant using a microstrip resonator is difficult.

To overcome the low quality factor of planar microstrip resonators, several research directions have been explored, such as dielectric resonators [13], [14], substrate-integrated waveguide (SIW) cavities [15], [16], microwave oscillators [17], and microwave-active resonator-based sensors [18], [19]. A high quality factor is achieved for the dielectric resonator by using a material with an extremely low dielectric loss. For this reason, the dielectric resonator is highly sensitive to samples with a small volume, but this scheme is bulky and quite expensive. The SIW cavity is constructed within a substrate by adding an upper conductor above a bottom conductor and caging the structure with plates via rows on both sides. This cavity is smaller in volume and less expensive than the dielectric resonator but has the disadvantage of storing the strongest energy at the center. Since the highest energy is stored at the center of the cavity, the target material must be located at the center to increase the sensitivity. These factors make reaction with the target material and replacement of impaired sensing materials in the SIW cavity difficult. In contrast, the microwave oscillator and active resonator consist of a planar microstrip resonator and an active circuit. Therefore, these sensors exhibit not only a high quality factor but also all the advantages of a planar microstrip resonator. By satisfying oscillation conditions, oscillation occurs near a single frequency. However, the output power of the oscillator is difficult to predict, and only deviations in the oscillation frequency can be used for the sensor. This means that achieving simultaneous detection of various variables is not easy. The microwave active resonator is similar to the microwave oscillator. However, it prevents oscillation by controlling the loop gain. Therefore, a microwave-active resonator can be used to measure multiple variables simultaneously with a high quality factor.

For these reasons, a relative humidity monitoring sensor based on an active resonator is proposed in this paper. The modified double split-ring resonator (DSRR) is used as a passive core in the active resonator. PEDOT:PSS is deposited in the gap of the outer ring. An active feedback loop is formed at the feed line of the passive core resonator by connecting the input to the base terminal and the output to the collector terminal of a bipolar junction transistor (BJT). The loss of the DSRR is compensated through integration with the active feedback loop, and the overall quality factor is improved 90-fold. The proposed sensor immediately detects the relative humidity and shows excellent performance compared to a commercial sensor as well as the sensor proposed in a previous work by our group [20].

II. SENSOR DESIGN

A. PASSIVE CORE RESONATOR DESIGN

In this work, a modified DSRR is used as a passive core resonator. The operating frequency of the resonator is chosen to be 2.45 GHz, which is an unlicensed industrial-scientific medical (ISM) band. The operating frequency of the DSRR can be determined as [21]:

$$\begin{aligned} \omega &= \sqrt{\frac{1}{2a_0 L_{res.} C_{res.}}} \\ L_{res.} &= L_{eff} + L_m \\ C_{res.} &= (C_{g1} + C_{g2}) || (C_{d1} + C_{d2}) \end{aligned} \tag{1}$$

where a_0 is the distance between the center of the resonator and the middle of the inner and outer squares, as illustrated in Figure 1 (a). L_{eff}, L_m, C_{g1}, C_{g2}, C_{d1} and C_{d2} are the effective inductance obtained from a_0, the mutual inductance between the two squares, the capacitances at the split of each ring, and the capacitances between the two rings. Here, the physical length and gap are determined to satisfy the above equation, as indicated in Figure 1 (a). The physical length and gap are set to the same values used in a previous study [20]. However, an additional feeding path has been

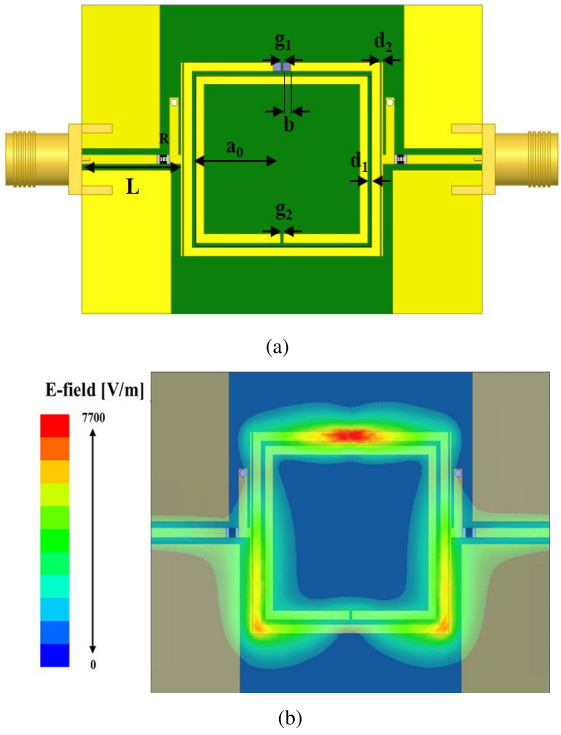

FIGURE 1. Design properties of the resonator and its simulation result. (a) Dimensions of the passive core resonator (L = 12.35 mm, a_0 = 11.5 mm, b = 1 mm, d_1 = 0.5 mm, d_2 = 0.2 mm, g_1 = 0.2 mm, g_2 = 0.3 mm, and R = 100 Ω). (b) Simulated result of the electric field distribution at the resonance frequency (1.5 mm above the substrate).

formed at the feeding line of the DSRR for connection with an active circuit, and an additional lumped resistor is attached to the side of the feeding path to prevent the active resonator from oscillating.

The sensing region of the resonator is set to the area of the maximum electric field to enhance the sensitivity. By depositing PEDOT:PSS in the maximum electric field region, the chemical reaction between PEDOT:PSS and water vapor can be detected with high resolution. For the DSRR, the sensing region is the gap in the outer ring, as shown in Figure 1 (b). In the sensing region of the resonator, a well structure is formed for stable deposition. The well structure is constructed by using a copper line and a mask layer. The mask layer is incorporated on the substrate, covering all parts except for the copper line and the sensing region. Since PEDOT:PSS is a conductive material, the copper line can be replaced with a PEDOT:PSS film by deposition on the well structure.

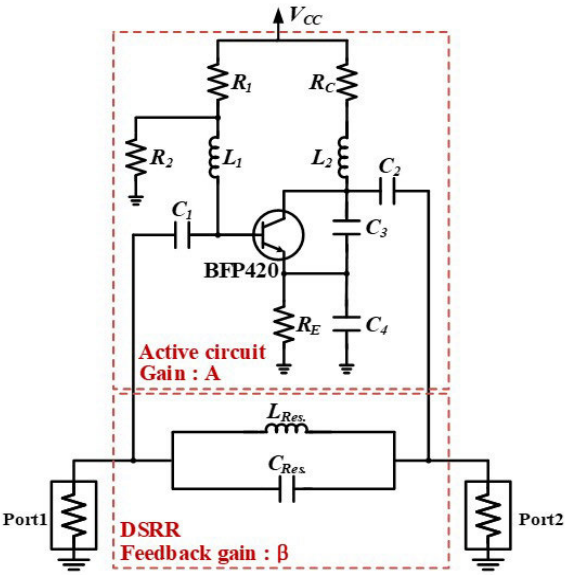

FIGURE 2. Conceptual diagram of the proposed active resonator.

B. ACTIVE FEEDBACK CIRCUIT DESIGN

To increase the quality factor of the DSRR, an active transistor is integrated. The BJT and the DSRR are vertically interconnected via holes. The input of the DSRR is connected to the base terminal, and the output is connected to the collector terminal to form an active feedback loop, as shown in Figure 2. The active resonator is designed as follows:

$$\begin{aligned} |S_{21}| &= G = |\beta A| < 1 \\ \angle S_{21} &= \angle \beta A = 2\pi n \end{aligned} \tag{2}$$

where β and A are the gains of the amplifier and feedback loop, respectively. G is the overall loop gain, which is the same as the transmission coefficient (S_{21}) of the active resonator, and n is an integer.

Similar to the Barkhausen condition used to determine the oscillation frequency, the phase of the active feedback loop is an integer multiple of 360° to compensate for the losses. However, the gain of the active feedback loop should be determined to prevent undesired oscillation. The active circuit is based on a common emitter circuit, and the voltage is supplied by a power-dividing circuit. The supplied voltage is set to 3 V and divided between the collector terminal and the base terminal. The BJT is biased at a base current of 174 μ A and a collector-emitter voltage of 1.54 V, with a collector current of 16 mA.

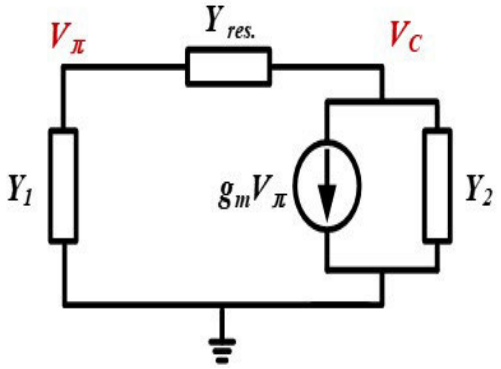

FIGURE 3. Simplified circuit model of the proposed active resonator.

C. ACTIVE RESONATOR DESIGN

The simplified equivalent circuit model of the proposed active resonator is shown in Figure 3. To determine the resonance frequency, the circuit model is simplified as follows: Since the resonance is determined by the reactance, all resistors are ignored in the circuit model. Moreover, the DC-blocking capacitors (C_1, C_2), which exhibit zero impedance at the resonance frequency, are not considered. Similarly, parasitic values, such as the depletion capacitance (C_μ) and diffusion capacitance (C_π), all of which are much lower than the lumped circuit values, are ignored in the calculations. The RF choke inductors (L_1, L_2), which exhibit open circuit characteristics at the microwave frequency, are also not considered in the calculations. The remaining lumped parameters can be converted into an admittance voltage matrix that satisfies Kirchhoff's current law (KCL). The KCL of each voltage node can be described as follows:

$$\begin{bmatrix} Y_1 + Y_{res.} & -Y_{res.} \\ g_m - Y_{res} & Y_{res.} + Y_2 \end{bmatrix} \begin{bmatrix} V \\ V_C \end{bmatrix} = \begin{bmatrix} 0 \\ 0 \end{bmatrix} \tag{3}$$

Since the voltages of the base and the collector are nonzero, the determinant of the admittance matrix should be zero for any possible solutions. The determinant of the admittance matrix is as follows:

$$(Y_1 + Y_{res.})(Y_2 + Y_{res.}) + g_m Y_{res.} - Y_{res.}^2 = 0 \tag{4}$$

By substituting the circuit values for the Y parameters into the the above equation, it can be divided into real and imaginary parts.

Real part:

$$-\omega^2 C_4 C_{res.} + \frac{C_4}{L_{res.}} - \omega^2 C_3 C_4 - \omega^2 C_3 C_{res.} - \frac{C_3}{L_{res.}} = 0 \tag{5}$$

Imaginary part:

$$\omega C_{res.} G_E - \frac{G_E}{\omega L_{res.}} + \omega C_3 G_E + \omega g_m C_{res.} - \frac{g_m}{\omega L_{res.}} = 0 \tag{6}$$

As both the real and imaginary parts equal zero, the resonance frequency of the active resonator can be derived as follows:

$$\omega = \sqrt{\frac{G_E + g_m}{L_{res.}((g_m + G_E)C_{res.} + C_3 G_E)}} = \sqrt{\frac{C_3 + C_4}{L_{res.}(C_{res.}C_4 + C_{res.}C_3 + C_3 C_4)}} \tag{7}$$

Moreover, by using Eq. 7, the relationship between the two feedback control capacitors (C_3, C_4) can be derived as follows:

$$\frac{C_3}{C_4} = g_m \tag{8}$$

III. HUMIDITY SENSING MECHANISM

In a humid environment, water molecules are adsorbed onto the surface of PEDOT:PSS. PEDOT:PSS reacts with water molecules, which causes changes in the intrinsic characteristics, including the morphological, physical and chemical properties. First, diffusion of water vapor into the deposited PEDOT:PSS film causes morphological deformation [22]. Water molecules are directly adsorbed onto the PSS sulfonic acid group as follows:

$$H_2O + PSS(HSO_3) \rightarrow H_3O^+ + PSS(SO_3^-) \tag{9}$$

The adsorbed water molecules interfere with the hydrogen bonding between the PSS molecules, which increases the size of the film. Moreover, hydrogen bonding between adsorbed water molecules and water vapor molecules accelerates water molecule sorption and induces more film swelling.

Second, diffusion of water vapor into the deposited PEDOT:PSS film causes a change in the effective dielectric constant [23]. Since water molecules have a high dielectric constant ($\epsilon_r = 80$), the effective dielectric constant determined by the filling factor of the surrounding material is highly influenced by the relative humidity. As the relative humidity increases, the proportion of the filling factor corresponding to water vapor is increased relative to that corresponding to dry air, thereby increasing the effective dielectric constant.

Third, diffusion of water vapor into the deposited PEDOT:PSS film causes a change in the chemical structure of PEDOT:PSS. PEDOT:PSS has a two-chemical-conformation structure according to the two resonance structures of PEDOT. Since the quinoid structure has delocalized ions,

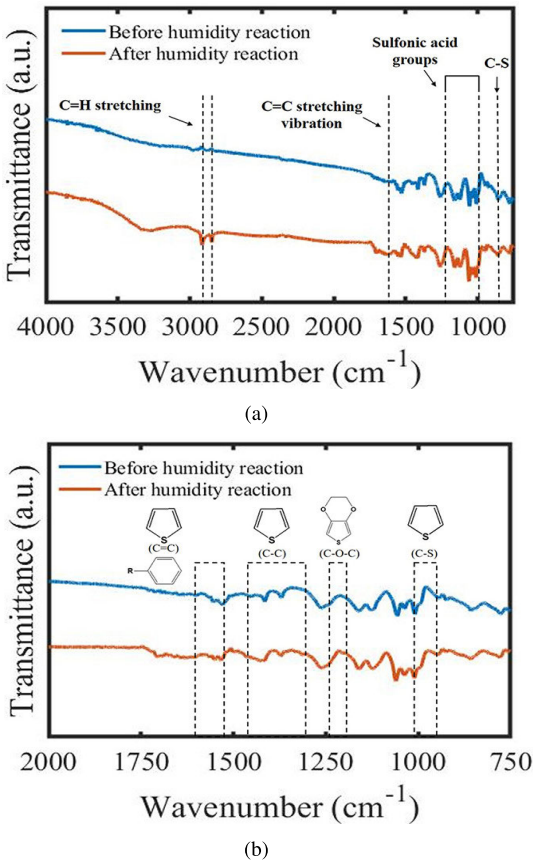

FIGURE 4. FT-IR spectra of the deposited PEDOT:PSS film. (a) Full spectral region. (b) Enlargement of the 2000-750 cm^{-1} region.

it has a higher conductivity than the benzoid structure. Pristine PEDOT:PSS has both benzoid and quinoid structures. However, when organic compounds with specific chemical properties are added, the benzoid structures are transformed into quinoid structures. The additives must have at least two polar groups in the molecule and be capable of forming hydrogen bonds with the PSS of PEDOT:PSS [24], [25]. The chemical reaction with these additives causes localized ions to become delocalized, which increases the electron density and leads to high conductivity. These mechanisms were verified using Fourier transform infrared (FT-IR) spectroscopy, as shown in Figure 4. The FT-IR spectrum of PEDOT:PSS changed as PEDOT reacted with humidity and changed from a benzoid structure to a quinoid structure. Figure 4 (a) shows the full spectral region of PEDOT:PSS [26]. The peaks at 2992 and 2851 cm^{-1} correspond to C-H symmetric and asymmetric stretching vibration of the PSS. The other peaks are from the PEDOT chain. The peaks at 1520 and 1307 cm^{-1} are assigned to the C-C and C=C stretching vibration of the thiophene ring, respectively. The peaks at 970, 916, and 822 cm^{-1} are assigned to stretching of the C-S bond in the thiophene ring. For a detailed analysis of the structural change of PEDOT, the 2000 - 750 cm^{-1} region is enlarged [27]. The results show that the position of the asymmetric C=C band shifts from 1514 cm^{-1} to 1528 cm^{-1}. The position of the

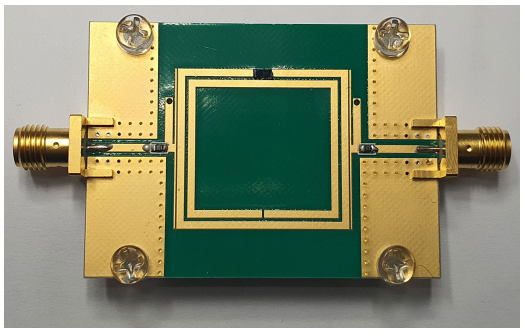

(a)

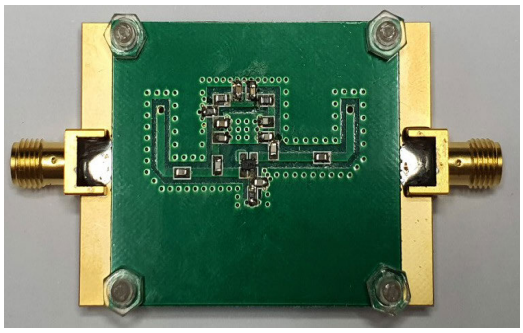

(b)

FIGURE 5. Fabricated sensor. (a) Top view of the proposed sensor (DSRR). (b) Bottom view of the proposed sensor (active circuit).

C-C stretching band shifts from 1365 cm^{-1} to 1375 cm^{-1}. However, the C-O-C vibration peak of the ethylenedioxy ring and the C-S vibration peak of the thiophene ring exhibit no significant differences, which can be interpreted based on the two resonance structures of PEDOT.

IV. FABRICATION OF THE SENSOR AND EXPERIMENTAL SETUP

A. FABRICATION OF THE ACTIVE RESONATOR

The proposed resonator is fabricated on a printed circuit board (PCB) substrate, which has a dielectric constant (ϵ_r) of 6.15 and a loss tangent (tanδ) of 0.0028, with a thickness of 0.762 mm. Surface mount device (SMD) resistors of 100 Ω are attached at both the input and output ports to prevent the active resonator from oscillating. The DSRR is vertically interconnected to the active circuit via holes, and they share a common ground plane in the middle layer to reduce the volume of the sensor. Figure 5 (a) shows the fabricated DSRR, which serves as the sensing layer of the proposed sensor. Figure 5 (b) shows the active circuit layer, which improves the quality factor of the sensing layer. The dimensions of the top and bottom layers are approximately 50 mm × 35 mm and 41 mm × 35 mm, respectively. Each layer is mechanically fixed by acrylic screws to prevent misalignment between the top and bottom layers.

B. SENSING MATERIAL DEPOSITION

An organic conducting polymer, PEDOT:PSS film, is used as a sensing material that chemically reacts with water molecules at room temperature. The solid content of the PEDOT:PSS solution used in this work is 1.1 wt%, and the weight ratio of PEDOT to PSS is 1:2.5. To increase the electrical conductivity of the PEDOT:PSS film, a typical dimethyl sulfoxide (DMSO) doping procedure is followed. DMSO is added to the aqueous PEDOT:PSS solution (5.0 v/v%) and stirred gently at room temperature. Then, the solution is filtered using a syringe filter (0.45 μm pore-size nylon membrane).

The PEDOT:PSS films are deposited as follows. First, the substrate is exposed to an oxygen plasma to improve the adhesion between the PEDOT:PSS film and the sensor. Second, polyimide tape is attached to the surrounding sensing regions of the sensor as a shield to prevent the PEDOT:PSS from overflowing. Then, the PEDOT:PSS solution is filled into the well structure by the drop-casting method, and the bar-coating technique is used to stabilize the roughness. Finally, the sensor is heated on a hot plate at 100°C to remove the water vapor remaining in the PEDOT:PSS.

To confirm the deposition of PEDOT:PSS on the substrate, several measurements are conducted. First, atomic force microscopy (AFM) is utilized to identify the roughness of the deposited PEDOT:PSS film. Figure 6 (a) shows that the PEDOT:PSS film has a maximum roughness of 10.7 nm and an average roughness of 1.933 nm, which means that it is deposited uniformly.

Second, scanning electron microscopy (SEM) is employed to evaluate the morphology of the deposited PEDOT:PSS film. The measurement is performed with a working distance of 8 mm, an acceleration voltage of 12.0 kV, and a magnification of 500. Figure 6 (b) shows the surface of the PEDOT:PSS film, which has few grains and elongated structures, indicating a good film forming capability.

Moreover, X-ray photoelectron spectroscopy (XPS) survey spectra of the deposited PEDOT:PSS film are also obtained, as shown in Figure 7. In contrast to AFM and SEM, XPS is a surface-sensitive technique that analyzes chemical bonds. PEDOT:PSS consists of PEDOT and PSS and contains one sulfur atom per repeat unit. However, the binding energies of PEDOT and PSS are different because PEDOT contains the thiophene ring and PSS includes the sulfonate moiety. Using these characteristics, PEDOT and PSS can be distinguished in the S(2p) spectra, and the composition of PEDOT:PSS can be determined by XPS. In Figure 7, the sulfur signal at the higher binding energy (167.7 eV) comes from PSS because the three electronegative oxygen atoms withdraw electron density from the sulfur atom. The sulfur signals at the lower binding energies (163.4 and 164.4 eV) are attributed to PEDOT [28].

C. EXPERIMENTAL SETUP

The performance of the proposed sensor is verified in a well-controlled environment chamber at 25 °C, as illustrated in Figure 8. Additionally, a commercial sensor is placed inside the chamber to investigate the accuracy by comparing the measured results. The proposed sensor is measured with

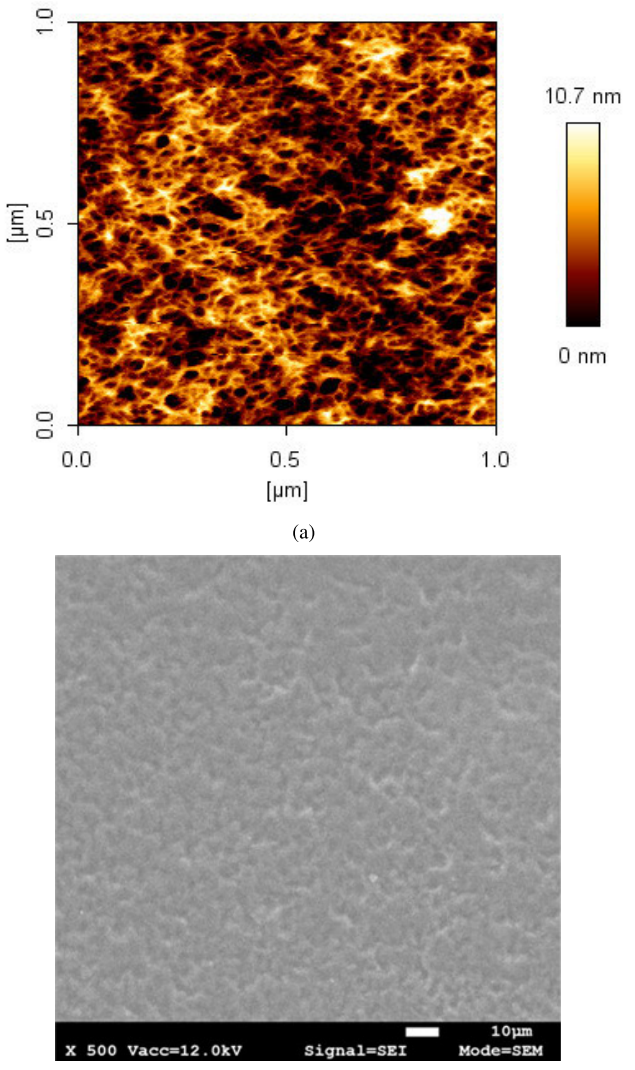

FIGURE 6. Morphologies of the deposited PEDOT:PSS film. (a) AFM image. (b) SEM image.

a vector network analyzer (VNA), and the measured data are sent to a computer every 0.5 seconds. The commercial sensor is connected to a microcontroller board, and the board also sends data to a computer every 0.5 seconds. Before the measurement, pure air gas is injected into the chamber to remove impurities. Then, water vapor is injected by the water vapor controller, and the humidity is controlled in the range from 30% to 85%.

V. RESULTS AND DISCUSSION

A. FREQUENCY RESPONSE OF THE PROPOSED SENSOR

The simulated and measured frequency responses (S_{21}) of the passive core resonator are presented in Figure 9. The S_{21} at the resonance frequency is set to -21 dB for oscillation prevention and stable operation. After depositing the PEDOT:PSS on the resonator, the resonance frequency is shifted to a lower frequency, from 2.45 GHz to 2.4 GHz. This occurs because PEDOT:PSS is a conductive material, and the deposition of the PEDOT:PSS film causes an increase in the

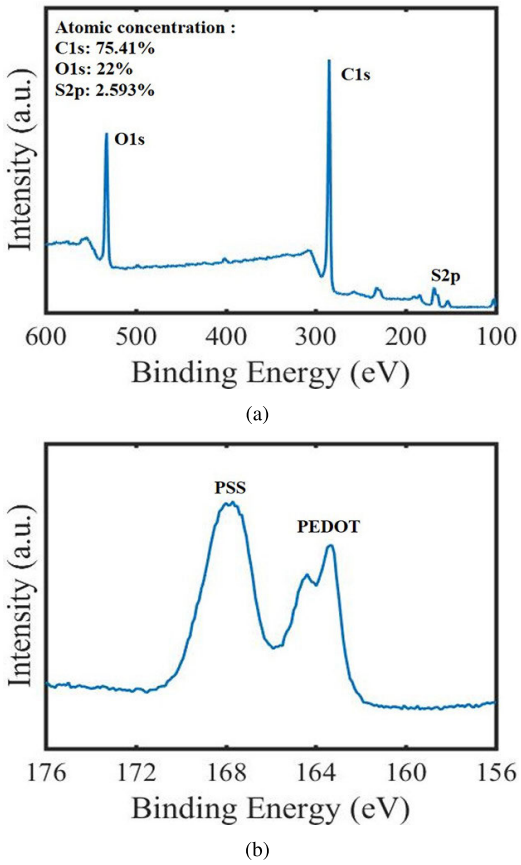

FIGURE 7. XPS spectra of the deposited PEDOT:PSS film. (a) XPS general scan. (b) Sulfur S(2p) spectra scan.

capacitance (C_{g1}). Thus, the resonance frequency is shifted slightly to a lower frequency. Additionally, S_{21} is decreased from -21 dB to -23 dB because although PEDOT:PSS is a conductive material, the conductivity is not as high as that of a metal. The slight difference between the measurement and the simulation is due to the additional transmission line length, including the connector, and the fabrication error.

The simulated and measured S_{21} frequency responses of the proposed active resonator are shown in Figure 10. The quality factor of the proposed sensor is greatly improved by associating it with an active circuit. The quality factors obtained from the measurement and simulation are approximately 2887 and 5056, respectively. The active resonator is operated at 2.4 GHz with an S_{21} of -8.9 dB at a humidity of 30%. As studied in previous work [20], the S_{21} of the sensor increases as the humidity increases. Therefore, to prevent oscillation, the S_{21} of the proposed sensor must be less than 0 dB even if the relative humidity increases to the maximum value in the range. For this reason, the margin for the proposed sensor to prevent oscillation is approximately 9 dB.

B. VERIFICATION OF THE PERFORMANCE OF THE PROPOSED SENSOR

The performance of the sensor is evaluated along with its repeatability and stability. The repeatability of the sensor is tested by controlling the humidity in real time in the range

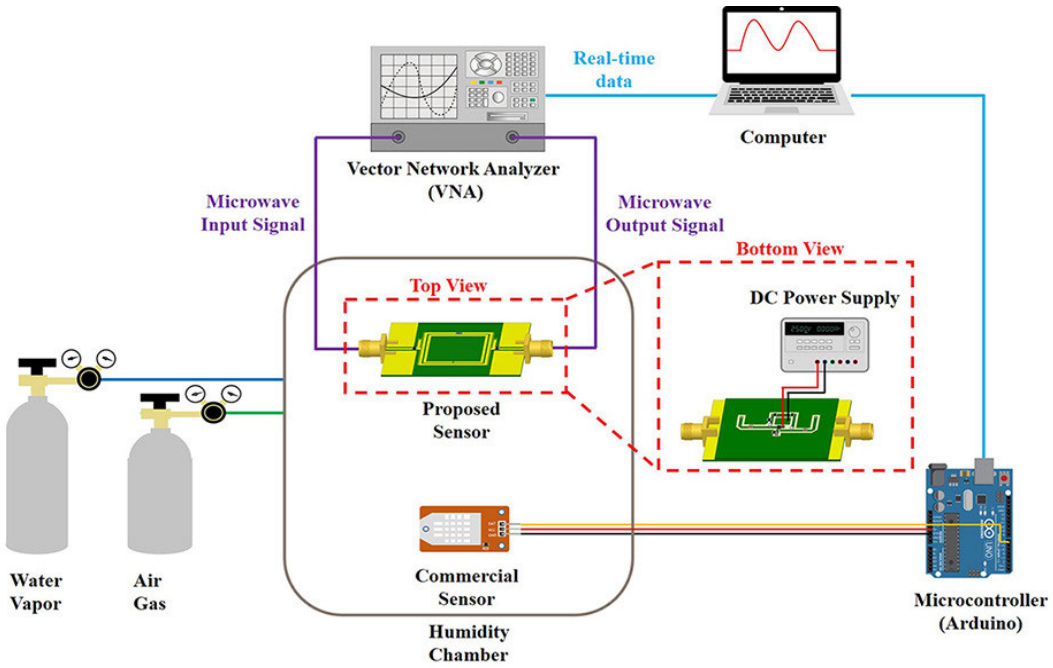

FIGURE 8. Measurement setup for relative humidity detection.

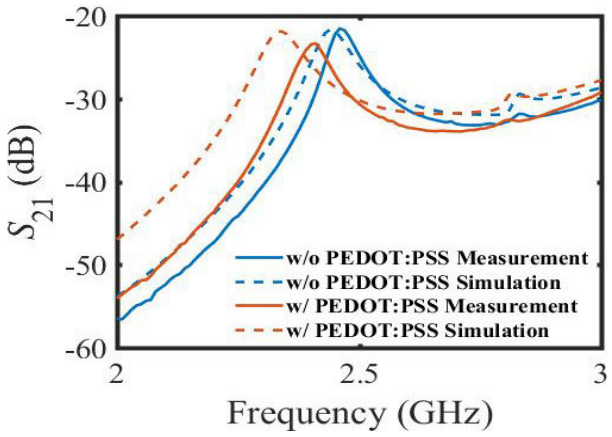

FIGURE 9. S_{21} results of the passive core resonator before and after PEDOT:PSS deposition.

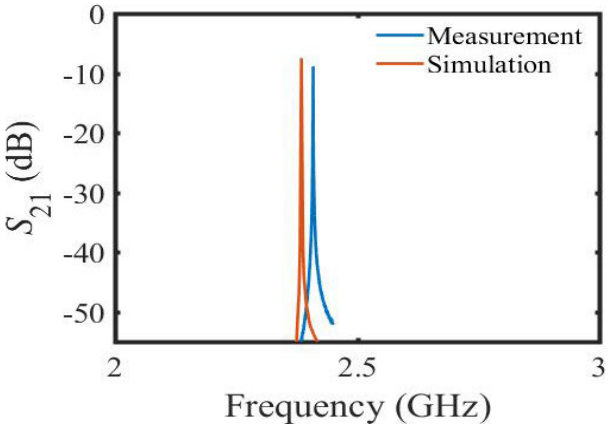

FIGURE 10. Frequency response of the active resonator with deposited PEDOT:PSS.

from 30% to 85%. The test consists of ten cycles, with each cycle lasting 60 s. In each cycle, half of the cycle is designated for injection of water vapor, while the other half is for ventilation. The stability of the sensor is tested by multiple measurements. Five samples with separately deposited PEDOT:PSS films are prepared for testing, and each sample is measured six times.

To quantitatively analyze the performance of the proposed humidity sensor, the following parameters are defined:

$$\begin{aligned} \Delta S_{21} &= S_{21,Humidity} - S_{21,30\%} \quad \text{(dB)} \\ \Delta F &= F_{Humidity} - F_{30\%} \quad \text{(MHz)} \end{aligned} \tag{10}$$

where S_{21} is the transmission coefficient at the resonance frequency. $S_{21,Humidity}$ and $F_{Humidity}$ are the values when the sensor reacts to humidity. $S_{21,30\%}$ and $F_{30\%}$ are the reference values when the humidity is the lowest (30%). Here, ΔS_{21} and ΔF are the differences in the transmission coefficient and resonance frequency, respectively.

Figure 11 shows the measurement results, demonstrating the repeatability of the proposed sensor. The repeatability test is conducted under extreme conditions where the humidity repeatedly changes from 30% to 85%. The blue line exhibits the results of the proposed sensor, while the red line exhibits the relative humidity measured by the commercial humidity sensor. As the humidity varies, ΔS_{21} and ΔF deviate simultaneously and show the possibility of realizing a real-time sensor. As the humidity increases, ΔS_{21} increases by 3.58 dB, while ΔF decreases by 8.85 MHz. Therefore, the results

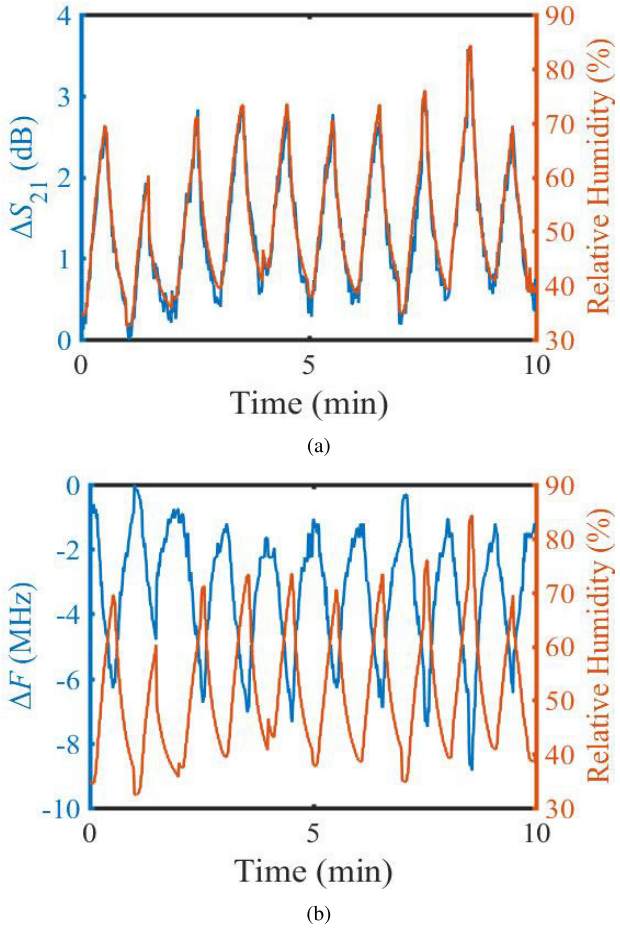

FIGURE 11. Measurement results for verifying the operating range. (a) ΔS_{21} deviation. (b) ΔF deviation.

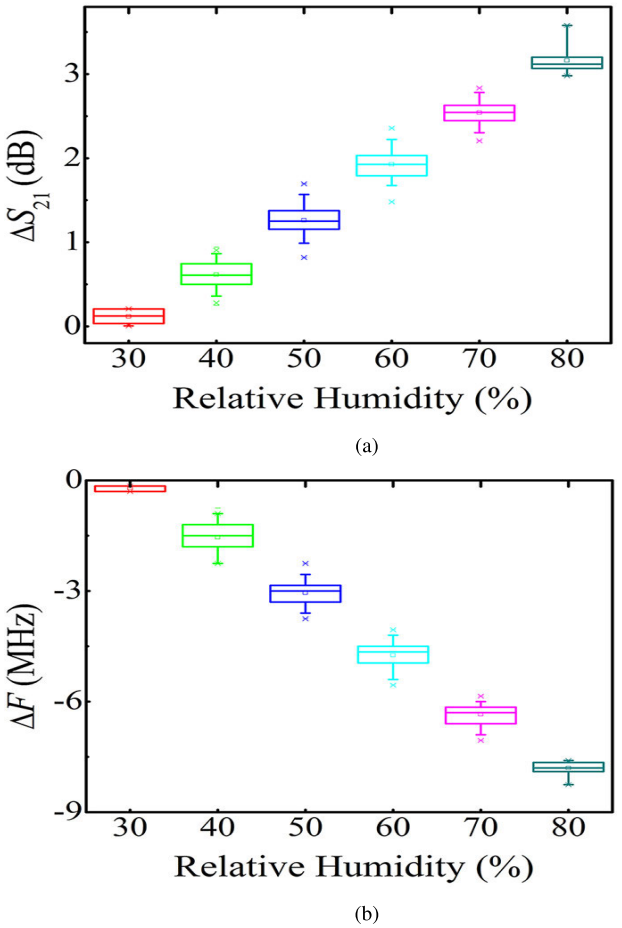

FIGURE 12. Statistical results of the proposed sensor. (a) ΔS_{21} deviation. (b) ΔF deviation.

TABLE 1. Box and whisker plot values of ΔS_{21}.

Relative Humidity	ΔS_{21} (dB)				
	Upper whisker	Upper quartile	Median	Lower quartile	Lower whisker
30	0.210	0.206	0.117	0.035	0.005
40	0.865	0.745	0.614	0.500	0.360
50	1.568	1.376	1.259	1.156	0.989
60	2.222	2.033	1.928	1.791	1.675
70	2.781	2.628	2.542	2.446	2.302
80	3.579	3.200	3.161	3.067	2.980

TABLE 2. Box and whisker plot values of ΔF.

Relative Humidity	ΔF (MHz)				
	Upper whisker	Upper quartile	Median	Lower quartile	Lower whisker
30	-0.150	-0.150	-0.200	-0.300	-0.300
40	-0.900	-1.200	-1.547	-1.800	-2.250
50	-2.550	-2.850	-3.050	-3.300	-3.600
60	-4.200	-4.500	-4.739	-4.950	-5.400
70	-6.000	-6.150	-6.346	-6.600	-6.900
80	-7.600	-7.650	-7.807	-7.900	-8.250

show that the proposed sensor operates stably under repetitive conditions and has an outstanding repeatable response when the humidity is in the range between 30% and 85%.

Figure 12 shows the measurement results used to verify the stability of the proposed sensor. The statistical distribution of the measured data is shown using a box and whisker plot. Five important items are used for the plot: upper whisker, upper quartile, median, lower quartile, and lower whisker. The upper and lower quartiles are the maximum and minimum of the box plot, representing 75% and 25% of the data distribution. The upper and lower whiskers indicate values corresponding to 1.5 times the upper or lower quartiles. The data outside the whisker range are considered outliers and are ignored in the analysis. The values of the five important items are summarized in Table 1 and Table 2. The whiskers for each humidity level as well as the boxes for each humidity level do not overlap. This means that the humidity is completely distinguishable for at least 10% variations and that the proposed sensor shows excellent stability. Therefore, the proposed active resonator-based sensor can clearly be

TABLE 3. Comparison of humidity sensors based on microwave components.

Component	Sensing Parameter	Humidity Range	Sensing Material	Sensitivity	Repeatability	Reference
Resonator	frequency	65-80%	Kapton HN Polyimide	200 kHz/RH	X	[29]
	frequency	0-80%	X	101 kHz/RH	X	[30]
Antenna	level, frequency	30-90%	Polyimide	4.95 mdB/RH, 181 kHz/RH 5.50 mdB/RH, 108 kHz/RH	X	[31]
	level	50-100%	PEDOT:PSS	0.2 dB/RH	O	[32]
RFID tag	frequency	25-90%	Polyimide	108 kHz/RH	X	[33]
	frequency	11.3-100%	Kapton HN	171.4 kHz/RH	X	[34]
Oscillator	frequency	0-40%	Polyimide	5 kHz/RH	X	[35]
	frequency	20-80%	PEDOT:PSS	67 kHz/RH	O	[17]
	frequency	5-65%	PANI/PVA	833 kHz/RH	O	[36]
Resonator	level, frequency	5-80%	PEDOT:PSS	2.4 mdB/RH, 470 kHz/RH	O	[20]
Active resonator	level, frequency	30-85%	PEDOT:PSS	**48.4 mdB/RH, 137 kHz/RH**	O	Current Work

used to detect humidity by measuring the changes in S_{21} as well as the resonance frequency.

In addition, the proposed sensor also demonstrates superior performance compared to those based on microwave components reported in other works, as summarized in Table 3. This table classifies humidity sensors based on the type of microwave component. The sensitivity is defined as follows:

$$\text{Sensitivity} = \frac{|\Delta S_{21}|}{|\Delta Humidity|} = \frac{|\Delta F|}{|\Delta Humidity|} \tag{11}$$

As shown in Table 3, only a few studies have proposed a sensor that can measure two variables. The most sensitive sensor based on changes in S_{21} is clearly the sensor proposed in this paper, while the most sensitive sensor based on frequency deviations is the sensor proposed in a previous work [20]. The ΔS_{21} of the proposed sensor is significantly increased to 24 times that reported in a previous work. However, the ΔF of the proposed sensor is decreased by one-third. This is because, in the case of a passive resonator, the resonance frequency is only affected by the resonator. However, in the case of an active resonator, the resonance frequency is determined by both the passive core resonator and the active circuit.

The changes in the characteristics of PEDOT:PSS can clearly be observed via the microwave electrical properties, S_{21} and resonance frequency. By measuring S_{21}, changes in chemical properties can be confirmed. Note that S_{21} is proportional to the conductivity. Thus, S_{21} will also increase when the conductivity increases proportional to a humidity increase, as confirmed in the measurements.

Furthermore, by measuring the resonance frequency, changes in the morphological and physical properties can be confirmed. The resonance frequency is inversely proportional to the square root of the capacitance of the PEDOT:PSS film (C_{g1}), and the capacitance is proportional to the effective dielectric constant, which is associated with physical properties. Moreover, the capacitance is proportional to the size of the deposited PEDOT:PSS film and inversely proportional to the gap size, which is related to morphological properties. The resonance frequency decreases as the effective dielectric constant increases when the humidity increases. Additionally, as the humidity increases, the size of the PEDOT:PSS film increases, and the gap size decreases, which also affects the reduction in the resonance frequency. This tendency is consistent with all the results shown above in that the resonance frequency shifts to a lower frequency. Therefore, the proposed sensor can simultaneously measure the changes in multiple characteristics by using a microwave-based circuit. Most importantly, the humidity can be detected with higher accuracy through measurement of both S_{21} and the resonance frequency.

VI. CONCLUSION

In this study, a relative humidity monitoring sensor was proposed based on a microwave-active resonator with a PEDOT:PSS film. A microwave-active resonator that operates at 2.4 GHz based on a positive feedback regenerative amplifier circuit has been introduced. The sensing system consists of two parts, a PEDOT:PSS-deposited passive core resonator and an active circuit, to achieve a high quality factor. By combining the two parts, the quality factor of the resonator increases 90-fold. The experimental results showed that the ΔS_{21} of the sensor increases by 3.58 dB and the resonance frequency of the sensor decreases by 8.85 MHz as the humidity increases from 30% to 85%. Thus, the variations in S_{21} and the resonance frequency clearly originate from the variations in the intrinsic characteristics of the PEDOT:PSS due to the relative humidity. Moreover, the proposed sensor could simultaneously measure changes in multiple intrinsic characteristics of the PEDOT:PSS by using a microwave-based circuit. The proposed sensor can clearly be utilized as a real-time high-sensitivity relative humidity monitoring sensor based on an electromagnetic field in the microwave region.

REFERENCES

[1] A. M. Nardes, M. Kemerink, M. M. de Kok, E. Vinken, K. Maturova, and R. A. J. Janssen, "Conductivity, work function, and environmental stability of PEDOT: PSS thin films treated with sorbitol," *Organic Electron.*, vol. 9, no. 5, pp. 727–734, Oct. 2008.

[2] C. Jang, J.-K. Park, G.-H. Yun, H. H. Choi, H.-J. Lee, and J.-G. Yook, "Radio-frequency/microwave gas sensors using conducting polymer," *Materials*, vol. 13, no. 12, p. 2859, Jun. 2020.

[3] Y. Seekaew, S. Lokavee, D. Phokharatkul, A. Wisitsoraat, T. Kerdcharoen, and C. Wongchoosuk, "Low-cost and flexible printed graphene–PEDOT:PSS gas sensor for ammonia detection," *Organic Electron.*, vol. 15, no. 11, pp. 2971–2981, Nov. 2014.

[4] G. U. Siddiqui, M. Sajid, J. Ali, S. W. Kim, Y. H. Doh, and K. H. Choi, "Wide range highly sensitive relative humidity sensor based on series combination of MoS_2 and PEDOT:PSS sensors array," *Sens. Actuators B, Chem.*, vol. 266, pp. 354–363, Aug. 2018.
[5] E. Bihar, Y. Deng, T. Miyake, M. Saadaoui, G. G. Malliaras, and M. Rolandi, "A disposable paper breathalyzer with an alcohol sensing organic electrochemical transistor," *Sci. Rep.*, vol. 6, no. 1, p. 27582, Sep. 2016.
[6] J.-E. Lim, S.-M. Lee, S.-S. Kim, T.-W. Kim, H.-W. Koo, and H.-K. Kim, "Brush-paintable and highly stretchable Ag nanowire and PEDOT:PSS hybrid electrodes," *Sci. Rep.*, vol. 7, no. 1, p. 14685, Dec. 2017.
[7] T.-G. Kang, J.-K. Park, B.-H. Kim, J. J. Lee, H. H. Choi, H.-J. Lee, and J.-G. Yook, "Microwave characterization of conducting polymer PEDOT: PSS film using a microstrip line for humidity sensor application," *Measurement*, vol. 137, pp. 272–277, Apr. 2019.
[8] M. Abdolrazzaghi, M. H. Zarifi, C. F. A. Floquet, and M. Daneshmand, "Contactless asphaltene detection using an active planar microwave resonator sensor," *Energy Fuels*, vol. 31, no. 8, pp. 8784–8791, Aug. 2017.
[9] C. Jang, J.-K. Park, H.-J. Lee, G.-H. Yun, and J.-G. Yook, "Temperature-corrected fluidic glucose sensor based on microwave resonator," *Sensors*, vol. 18, no. 11, p. 3850, Nov. 2018.
[10] C. Jang, J.-K. Park, H.-J. Lee, G.-H. Yun, and J.-G. Yook, "Non-invasive fluidic glucose detection based on dual microwave complementary split ring resonators with a switching circuit for environmental effect elimination," *IEEE Sensors J.*, vol. 20, no. 15, pp. 8520–8527, Aug. 2020.
[11] M. Abdolrazzaghi, M. H. Zarifi, and M. Daneshmand, "Wireless communication in feedback-assisted active sensors," *IEEE Sensors J.*, vol. 16, no. 22, pp. 8151–8157, Nov. 2016.
[12] J.-K. Park, Y. Hong, H. Lee, C. Jang, G.-H. Yun, H.-J. Lee, and J.-G. Yook, "Noncontact RF vital sign sensor for continuous monitoring of driver status," *IEEE Trans. Biomed. Circuits Syst.*, vol. 13, no. 3, pp. 493–502, Jun. 2019.
[13] J. Kim, A. Babajanyan, A. Hovsepyan, K. Lee, and B. Friedman, "Microwave dielectric resonator biosensor for aqueous glucose solution," *Rev. Sci. Instrum.*, vol. 79, no. 8, Aug. 2008, Art. no. 086107.
[14] N. Meyne, C. Cammin, and A. F. Jacob, "Accuracy enhancement of a split-ring resonator liquid sensor using dielectric resonator coupling," in *Proc. 20th Int. Conf. Microw., Radar Wireless Commun. (MIKON)*, Jun. 2014, pp. 1–4.
[15] E. Silavwe, N. Somjit, and I. D. Robertson, "A microfluidic-integrated SIW lab-on-substrate sensor for microliter liquid characterization," *IEEE Sensors J.*, vol. 16, no. 21, pp. 7628–7635, Nov. 2016.
[16] E. Massoni, G. Siciliano, M. Bozzi, and L. Perregrini, "Enhanced cavity sensor in SIW technology for material characterization," *IEEE Microw. Wireless Compon. Lett.*, vol. 28, no. 10, pp. 948–950, Oct. 2018.
[17] T.-G. Kang, J.-K. Park, G.-H. Yun, H. H. Choi, H.-J. Lee, and J.-G. Yook, "A real-time humidity sensor based on a microwave oscillator with conducting polymer PEDOT:PSS film," *Sens. Actuators B, Chem.*, vol. 282, pp. 145–151, Mar. 2019.
[18] M. H. Zarifi, S. Farsinezhad, K. Shankar, and M. Daneshmand, "Liquid sensing using active feedback assisted planar microwave resonator," *IEEE Microw. Wireless Compon. Lett.*, vol. 25, no. 9, pp. 621–623, Sep. 2015.
[19] M. H. Zarifi, A. Gholidoust, M. Abdolrazzaghi, P. Shariaty, Z. Hashisho, and M. Daneshmand, "Sensitivity enhancement in planar microwave active-resonator using metal organic framework for CO_2 detection," *Sens. Actuators B, Chem.*, vol. 255, pp. 1561–1568, Feb. 2018.
[20] J.-K. Park, T.-G. Kang, B.-H. Kim, H.-J. Lee, H. H. Choi, and J.-G. Yook, "Real-time humidity sensor based on microwave resonator coupled with PEDOT:PSS conducting polymer film," *Sci. Rep.*, vol. 8, no. 1, p. 439, Dec. 2018.
[21] C. Saha and J. Y. Siddiqui, "A comparative analyis for split ring resonators of different geometrical shapes," in *Proc. IEEE Appl. Electromagn. Conf. (AEMC)*, Dec. 2011, pp. 1–4.
[22] E. S. Muckley, J. Lynch, R. Kumar, B. Sumpter, and I. N. Ivanov, "PEDOT: PSS/QCM-based multimodal humidity and pressure sensor," *Sens. Actuators B, Chem.*, vol. 236, pp. 91–98, Nov. 2016.
[23] N. Koch, A. Vollmer, and A. Elschner, "Influence of water on the work function of conducting poly(3,4-ethylenedioxythiophene)/poly (styrenesulfonate)," *Appl. Phys. Lett.*, vol. 90, no. 4, Jan. 2007, Art. no. 043512.
[24] J. Ouyang, Q. Xu, C.-W. Chu, Y. Yang, G. Li, and J. Shinar, "On the mechanism of conductivity enhancement in poly(3,4-ethylenedioxythiophene): Poly(styrene sulfonate) film through solvent treatment," *Polymer*, vol. 45, no. 25, pp. 8443–8450, Nov. 2004.
[25] J. Ouyang, C.-W. Chu, F.-C. Chen, Q. Xu, and Y. Yang, "High-conductivity Poly(3,4-ethylenedioxythiophene): Poly(styrene sulfonate) film and its application in polymer optoelectronic devices," *Adv. Funct. Mater.*, vol. 15, no. 2, pp. 203–208, Feb. 2005.
[26] X. Wang, M. Li, G. Feng, and M. Ge, "On the mechanism of conductivity enhancement in PEDOT:PSS/PVA blend fiber induced by UV-light irradiation," *Appl. Phys. A, Solids Surf.*, vol. 126, no. 3, p. 184, Mar. 2020.
[27] E. Mitraka, M. J. Jafari, M. Vagin, X. Liu, M. Fahlman, T. Ederth, M. Berggren, M. P. Jonsson, and X. Crispin, "Oxygen-induced doping on reduced PEDOT," *J. Mater. Chem. A*, vol. 5, no. 9, pp. 4404–4412, 2017.
[28] Z. Zhu, C. Liu, H. Shi, Q. Jiang, J. Xu, F. Jiang, J. Xiong, and E. Liu, "An effective approach to enhanced thermoelectric properties of PEDOT: PSS films by a Des.Post-treatment," *J. Polym. Sci. Part B, Polym. Phys.*, vol. 53, no. 12, pp. 885–892, Jun. 2015.
[29] E. M. Amin and N. C. Karmakar, "Development of a low cost printable humidity sensor for chipless RFID technology," in *Proc. IEEE Int. Conf. RFID-Technologies Appl. (RFID-TA)*, Nov. 2012, pp. 165–170.
[30] H. El Matbouly, N. Boubekeur, and F. Domingue, "Passive microwave substrate integrated cavity resonator for humidity sensing," *IEEE Trans. Microw. Theory Techn.*, vol. 63, no. 12, pp. 4150–4156, Dec. 2015.
[31] Y.-H. Kim, K. Jang, Y. J. Yoon, and Y.-J. Kim, "A novel relative humidity sensor based on microwave resonators and a customized polymeric film," *Sens. Actuators B Chem.*, vol. 117, no. 2, pp. 315–322, 2006.
[32] S. Manzari, C. Occhiuzzi, S. Nawale, A. Catini, C. Di Natale, and G. Marrocco, "Humidity sensing by polymer-loaded UHF RFID antennas," *IEEE Sensors J.*, vol. 12, no. 9, pp. 2851–2858, Sep. 2012.
[33] K. Chang, Y. H. Kim, Y. J. Kim, and Y. J. Yoon, "Functional antenna integrated with relative humidity sensor using synthesised polyimide for passive RFID sensing," *Electron. Lett.*, vol. 43, no. 5, pp. 7–8, Mar. 2007.
[34] J. Virtanen, L. Ukkonen, T. Björninen, A. Z. Elsherbeni, and L. Sydänheimo, "Inkjet-printed humidity sensor for passive UHF RFID systems," *IEEE Trans. Instrum. Meas.*, vol. 60, no. 8, pp. 2768–2777, Aug. 2011.
[35] C. Bernou, D. Rebière, and J. Pistré, "Microwave sensors: A new sensing principle. Application to humidity detection," *Sens. Actuators B Chem.*, vol. 68, no. 1, pp. 88–93, 2000.
[36] M. Abdolrazzaghi, F. Hariri, M. Chu, H. Naguib, and M. Daneshmand, "Relative humidity sensing using PANI/PVA integrated with feedback oscillator circuit," in *Proc. IEEE Sensors*, Oct. 2019, pp. 1–4.

JIN-KWAN PARK (Graduate Student Member, IEEE) was born in Seoul, South Korea. He received the B.S. degree in electronics and electrical engineering from Dongguk University, Seoul, in 2014. He is currently pursuing the Ph.D. degree in electrical and electronics engineering with Yonsei University, Seoul. His main research interests include RF-based sensors, such as vital-sign, humidity, glucose, and gas sensors, and microwave/millimeter-wave components/systems.

CHOROM JANG (Graduate Student Member, IEEE) was born in Incheon, South Korea. She received the B.S. degree in electronics engineering from Seokyeong University, Seoul, South Korea, in 2017. She is currently pursuing the Ph.D. degree in electrical and electronics engineering with Yonsei University, Seoul. Her main research interests include RF-based sensors, such as glucose, vital-sign, and pressure sensors, and microwave components/systems.

GI-HO YUN was born in Jeonju, South Korea. He received the M.S. and Ph.D. degrees in electronics engineering from Yonsei University, Seoul, South Korea, in 1986 and 1999, respectively. From 1985 to 1997, he was with Samsung Electronics and Samsung Electro-Mechanics. Then, he was with Honam University, Gwangju, South Korea, from 1997 to 2008. He is currently a Professor with the Division of Information and Communication Engineering, Sungkyul University, Anyang, South Korea. He is also with the Advanced Computational Electromagnetic Laboratory, Yonsei University. His current research interests include active and passive circuitry in the RF/MW frequency and various sensors to detect vital signals and biosignals in the human body.

HEE-JO LEE (Member, IEEE) received the Ph.D. degree in electrical and electronics engineering from Yonsei University, Seoul, South Korea, in 2010. From March 2010 to March 2012, he worked with the Department of Electrical and Electronics Engineering, Yonsei University, and the Graphene Research Institute, Sejong University, Seoul, as a Postdoctoral Researcher. From April 2012 to August 2014, he worked with the Department of Mechanical Engineering and the Department of Electrical and Electronics Engineering, Yonsei University, as a Research Professor. Since September 2014, he has been an Assistant Professor with the Department of Physics Education, Daegu University. His main research interests include electromagnetic wave and field theory, RF/microwave bio- and gas- sensors, RF/microwave circuit modeling, the characterization of carbon nanomaterials, including graphene, graphene ribbons, and graphene oxide, and electromagnetic metamaterials for biosensing.

HYANG HEE CHOI received the Ph.D. degree in chemical engineering from Chosun University, Gwangju, South Korea, in 1998. From January 2001 to December 2001, she worked at the University of Massachusetts, Amherst, as a Postdoctoral Researcher. From March 2005 to February 2010, she worked at the Yonsei Nanomedical Core Research Center, Yonsei University, South Korea, as a Research Professor. Since March 2010, she has been a Research Professor with the Institute of Engineering Research, Yonsei University. Her main research interests include hazardous gas detection and sensor materials, organic and inorganic synthesis, the applications of nanomaterials, and thermal characterization using conductive polymers.

JONG-GWAN YOOK (Senior Member, IEEE) was born in Seoul, South Korea. He received the B.S. and M.S. degrees in electronics engineering from Yonsei University, Seoul, in 1987 and 1989, respectively, and the Ph.D. degree from the University of Michigan, Ann Arbor, MI, USA, in 1996. He is currently a Professor with the School of Electrical and Electronics Engineering, Yonsei University. His main research interests include theoretical/numerical electromagnetic modeling and the characterization of microwave/millimeter-wave circuits and components, the design of radio frequency integrated circuits (RFICs) and monolithic microwave integrated circuits (MMICs), and the analysis and optimization of high-frequency high-speed interconnects, including the signal/power integrity (EMI/EMC), based on frequency- and time-domain full-wave methods. His research team recently developed various biosensors such as carbon nanotube RF biosensors for nanometer-size antigen-antibody detection and remote wireless vital signal monitoring sensors.